AGU PUBLICATIONS

JGR

Journal of Geophysical Research: Space Physics

RESEARCH ARTICLE
10.1002/2016JA023858

Special Section:
Magnetospheric Multiscale (MMS) mission results throughout the first primary mission phase

Observations of kinetic-size magnetic holes in the magnetosheath

S. T. Yao[1,2], X. G. Wang[3], Q. Q. Shi[1], T. Pitkänen[2], M. Hamrin[2], Z. H. Yao[4,5], Z. Y. Li[6], X. F. Ji[6], A. De Spiegeleer[2], Y. C. Xiao[1], A. M. Tian[1], Z. Y. Pu[7], Q. G. Zong[7], C. J. Xiao[6], S. Y. Fu[7], H. Zhang[8], C. T. Russell[9], B. L. Giles[10], R. L. Guo[11], W. J. Sun[11], W. Y. Li[12,13], X. Z. Zhou[7], S. Y. Huang[14], J. Vaverka[2], M. Nowada[1], S. C. Bai[1], M. M. Wang[1], and J. Liu[13]

[1]Shandong Provincial Key Laboratory of Optical Astronomy and Solar-Terrestrial Environment, Institute of Space Sciences, Shandong University, Weihai, China, [2]Department of Physics, Umeå University, Umeå, Sweden, [3]Department of Physics, Harbin Institute of Technology, Harbin, China, [4]Mullard Space Science Laboratory, University College London, Dorking, UK, [5]Laboratoire de Physique Atmosphérique et Planétaire, STAR Institute, Université de Liège, Liège, Belgium, [6]State Key Laboratory of Nuclear Physics and Technology, School of Physics, Peking University, Beijing, China, [7]School of Earth and Space Sciences, Peking University, Beijing, China, [8]Physics Department and Geophysical Institute, University of Alaska Fairbanks, Fairbanks, Alaska, USA, [9]Department of Earth, Planetary and Space Sciences, University of California, Los Angeles, California, USA, [10]NASA Goddard Space Flight Center, Greenbelt, Maryland, USA, [11]Key Laboratory of Earth and Planetary Physics, Institute of Geology and Geophysics, Chinese Academy of Sciences, Beijing, China, [12]Swedish Institute of Space Physics, Uppsala, Sweden, [13]State Key Laboratory of Space Weather, National Space Science Center, Chinese Academy of Sciences, Beijing, China, [14]School of Electronic Information, Wuhan University, Wuhan, China

Key Points:
- Magnetosheath kinetic-size magnetic holes are found with electron flow vortex caused by diamagnetic drift
- At the 90° pitch angle, the 34–66 eV electron flux decreased while 109–1024 eV electron flux increased inside the MHs
- Quasi-2-D EMHD soliton theory is applicable to the observations

Correspondence to:
Q. Q. Shi,
sqq@pku.edu.cn

Citation:
Yao, S. T., et al. (2017), Observations of kinetic-size magnetic holes in the magnetosheath, *J. Geophys. Res. Space Physics*, *122*, 1990–2000, doi:10.1002/2016JA023858.

Received 30 DEC 2016
Accepted 3 FEB 2017
Accepted article online 8 FEB 2017
Published online 23 FEB 2017

Abstract Magnetic holes (MHs), with a scale much greater than ρ_i (proton gyroradius), have been widely reported in various regions of space plasmas. On the other hand, kinetic-size magnetic holes (KSMHs), previously called small-size magnetic holes, with a scale of the order of magnitude of or less than ρ_i have only been reported in the Earth's magnetospheric plasma sheet. In this study, we report such KSMHs in the magnetosheath whereby we use measurements from the Magnetospheric Multiscale mission, which provides three-dimensional (3-D) particle distribution measurements with a resolution much higher than previous missions. The MHs have been observed in a scale of 10–20 ρ_e (electron gyroradii) and lasted 0.1–0.3 s. Distinctive electron dynamics features are observed, while no substantial deviations in ion data are seen. It is found that at the 90° pitch angle, the flux of electrons with energy 34–66 eV decreased, while for electrons of energy 109–1024 eV increased inside the MHs. We also find the electron flow vortex perpendicular to the magnetic field, a feature self-consistent with the magnetic depression. Moreover, the calculated current density is mainly contributed by the electron diamagnetic drift, and the electron vortex flow is the diamagnetic drift flow. The electron magnetohydrodynamics soliton is considered as a possible generation mechanism for the KSMHs with the scale size of 10–20 ρ_e.

1. Introduction

Magnetic holes (MHs), a structure with observable magnetic field depression, were first reported in the solar wind plasmas [*Turner et al*., 1977] and then widely observed in the interplanetary space [e.g., *Winterhalter et al*., 1994; *Zhang et al*., 2008, 2009; *Xiao et al*., 2010, 2014], the magnetosphere of comet [e.g., *Russell et al*., 1987], the planetary magnetosheath [e.g., *Tsurutani et al*., 1982, 1984; *Balogh et al*., 1992; *Violante et al*., 1995; *Bavassano-Cattaneo et al*., 1998; *Lucek et al*.,1999; *Walker et al*., 2002, 2004; *Joy et al*., 2006; *Soucek et al*., 2008; *Balikhin et al*., 2009; *Nowada et al*., 2009], and the magnetospheric cusp [*Shi et al*., 2009]. Spatial scales of these structures ranged from tens to thousands of ρ_i (proton gyroradius) with corresponding temporal scales from seconds to tens of minutes. Previous studies associated these holes with mirror instabilities [e.g., *Kaufmann et al*., 1970; *Tsurutani et al*., 1982; *Southwood and Kivelson*, 1993; *Fazakerley and Southwood*, 1994; *Chisham et al*., 1999; *Horbury et al*., 2004; *Joy et al*., 2006; *Zhang et al*., 2008, 2009; *Shi et al*., 2009; *Xiao et al*., 2010, 2011, 2014]. Other possible mechanisms, such as sheet-like equilibrium structures [*Burlaga and Lemaire*, 1978] and solitary waves [*Baumgärtel*, 1999; *Stasiewicz*, 2004] have also been applied to explain the formation of MHs.

Aforementioned observations were large magnetohydrodynamics (MHD) size MHs, and the applied theories were generally based on the MHD scales. For instance, the mirror instability is associated with the adiabatic bounce of the particle guide center in a slowly varying nonuniform background magnetic field. Thus, the

scale size of the mirror structure should exceed ρ_i substantially. However, for MHs with scale less than or of the order of ρ_i reported in the magnetospheric plasma sheet [*Ge et al*., 2011; *Sun et al*., 2012; *Sundberg et al*., 2015; *Gershman et al*., 2016; *Goodrich et al*., 2016], one has to use the kinetic scale instead of the MHD scale theory to study them. These kinetic-size magnetic holes (KSMHs) are observed both during geomagnetically quiet [*Sun et al*., 2012] and active times [*Ge et al*., 2011]. Based on the theory of electron magnetohydrodynamics (EMHD), a model of one-dimensional (1-D) slow-mode soliton has been developed to explain the KSMHs during quiet time [*Ji et al*., 2014]. *Yao et al*. [2016] calculated the propagating velocity of such holes. The velocity together with the amplitude and size fitted well with the theory of EMHD solitons. *Li et al*. [2016] extended this approach to quasi-2-D soliton model. Also, it was reported that KSMHs observed in the active plasma sheet were believed to be associated with tearing instabilities and dipolarization fronts energy dissipation [*Ge et al*., 2011; *Balikhin et al*., 2012]. In a recent particle-in-cell simulation, *Haynes et al*. [2015] presented a subproton scale magnetic hole, also named "electron vortex magnetic hole" (EVMH). This kind of structure was found in the simulation of decaying turbulences with a guide field and contained a population of electrons with a ring current formed by the mean azimuthal electron flow. *Roytershteyn et al*. [2015] also showed a similar result in the fully kinetic simulation of collisionless turbulence. Through analysis of electron properties and spatial size of the KSMHs in the plasma sheet, *Sundberg et al*. [2015] suggested that cylindrical-like and sheet-like MHs might be associated with EVMH and electron solitary wave, respectively. More recently, KSMHs with current surrounding it was observed in the plasma sheet [*Gershman et al*., 2016]. The current was carried by electrons with gyroradius larger than the thermal gyroradius but smaller than the current layer thickness, and it was thought to be responsible for the formation of the KSMHs. Similar currents around KSMHs in the plasma sheet were inferred by the analysis of electromagnetic field data and attributed to the $E \times B$ drift of electrons [*Goodrich et al*., 2016].

Previous works on KSMHs demonstrated that the structures were widely observed in the plasma sheet, with a duration of seconds and a scale size of hundreds of kilometers [*Ge et al*., 2011; *Sun et al*., 2012; *Sundberg et al*., 2015; *Gershman et al*., 2016; *Goodrich et al*., 2016]. In this study, we report a series of KSMHs in the magnetosheath. These structures are observed with a scale size of tens of kilometers and have a temporal duration of 0.1–0.3 s. High time resolution data have been used to study their characteristics. We introduce the data set in section 2, the plasma features of KSMHs in section 3, and the detailed analysis of electron flux and pitch angle distributions in section 4, followed by a summary and discussion section.

2. Data and Events

The Magnetospheric Multiscale (MMS) [*Burch et al*., 2016] spacecraft were launched in March 2015. Up to now the four satellites have been crossing the magnetopause numerous times and therefore provide us with a large amount of data for studying the characteristics of KSMHs in the magnetosheath. Particularly, we select events with burst mode Fluxgate magnetometer (FGM) data [*Russell et al*., 2016], during which the resolution is 7.8 ms. We also investigate burst mode Fast Plasma Investigation (FPI) data [*Pollock et al*., 2016]. The resolution of ions burst mode data is 150 ms and that of electrons is 30 ms. A total of 83 events from September 2015 to January 2016 in the magnetosheath are selected for our investigation. In order to compare with the soliton theory in section 5, 17 events with the scale size of 10–20 ρ_e (electron gyroradius, the typical magnitude of electron gyroradius in the magnetosheath is about 1 km) are selected in this work. The events are first identified by eye with the criterion of magnetic depression less than 1 s, and then selected with $B_{min}/B \leq 0.9$, $\delta \leq 2$ nT and $\omega \leq 15°$. Here B, B_{min}, and δ are, respectively, the average, minimum and standard deviation of magnetic field magnitudes within 5 s surrounding the center of the hole. The KSMHs duration is considered as the time interval between the leading and trailing edges of the MHs where the edges are defined by the decrease of B to $(B - \delta)$. And ω is the angle between the average magnetic field vectors before and after the magnetic depression in 5 times of KSMHs interval, indicating the field direction change over the event.

3. Plasma Features of KSMHs

A 1 min overview plot of a typical example of KSMH is shown in Figures 1a–1k. We show the magnetic field components, plasma parameters, and energy spectrums from MMS1 in the Geocentric Solar Ecliptic (GSE) coordinate system. The hole was observed at 14:59:34 UT and lasted for ~0.24 s. MMS was located

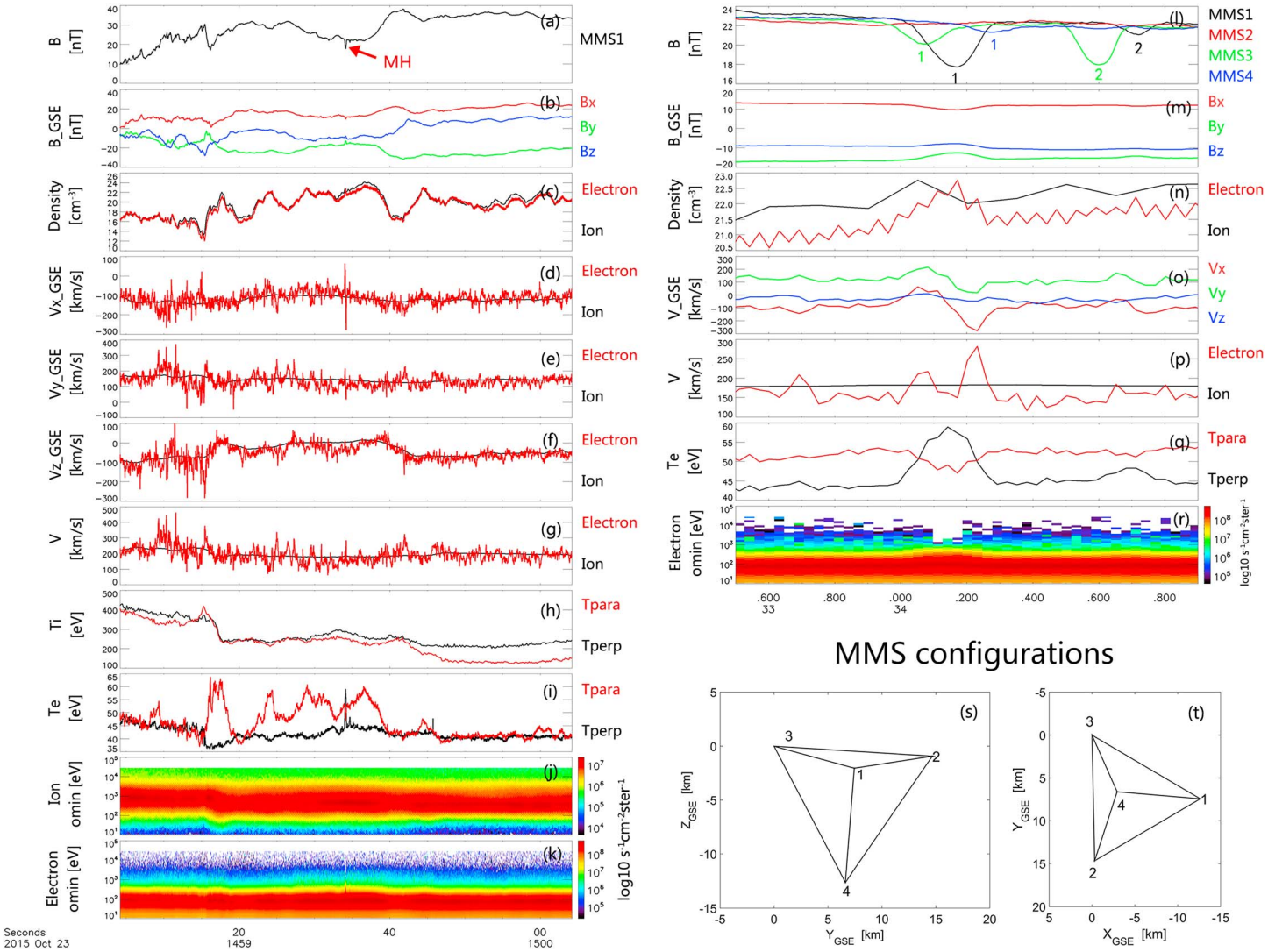

Figure 1. (a–k) Overview plots of magnetic field, ion and electron density, bulk velocity, temperature, and spectrograms in 1 min. (l) Details of magnetic field strength from MMS1–MMS4 in 1.5 s. The numbers "1" and "2" denote two magnetic holes. (m–r) Details of electron density, bulk velocity, temperature, and electron energy time spectrogram from MMS1. (s–t) MMS tetrahedron configuration.

at [7.6, 8.1, −0.8] R_E (Earth radius). The short duration makes the structure difficult to be identified in the 1 min overview plot. We determine that the hole was observed in the magnetosheath, based on the plasma parameters (number density, bulk velocity, and particle temperature) and the energy spectrum. Figures 1l–1r and 1s–1t present the details of the KSMHs and MMS tetrahedron configuration, respectively. During this time interval, MMS1 had the longest duration observation of this magnetic hole. It was also observed by MMS3 and MMS4 while no significant change of magnetic field magnitudes was seen by MMS2. We mark this hole as "1." Note that 0.5 s later, another hole was detected by MMS1 and MMS3. We mark it as "2." The time interval between the two events detected by MMS1 was almost the same as that by MMS3.

During the encounter with event 1, the magnetic field magnitude at MMS1 dropped about 6 nT, and the magnetic field vector changed from (13, −17, −11) nT to (10, −13, −8) nT. The angle between (13, −17, −11) nT and (10, −13, −8) nT is 1°. From Figure 1n, we can see that the electron number density increased inside the structure. The resolution of the ion number density is 0.15 s. Thus, it is not enough to interpret the ion features for such small structures with duration of 0.24 s. Figures 1o–1p show the vector of electron bulk velocity in the GSE coordinate system and the magnitude of electron and ion bulk speeds. Bipolar

electron flow signatures were observed for both V_x and V_y and were centered near the dip of the MH. Figure 1p, together with Figures 1d–1g show a distinctive variation in the electron flow. The resolution of the ion data (0.15 s) does not allow us to resolve any changes in the ion bulk flows within the hole. However, due to the small spatial size of the hole, we expect that the ion bulk flow is not affected by it (similar conclusion in *Eastwood et al.* [2016]). Our data in Figures 1d–1g do not contradict this conclusion. Furthermore, we find that the electron temperature anisotropy significantly increased inside the hole. The perpendicular electron temperature increased to 60 eV, while the parallel temperature dropped to 47 eV (reference to Figure 1q). In event 2, similar features of the temperature, velocity, and magnetic field are found. In the following, we focus on event 1.

We transformed the electron flow velocity vectors into an *LMN* coordinate system, which is determined by the magnetic field minimum variance analysis (MVA) [*Sonnerup and Scheible*, 1998] using magnetic field data of MMS1. $L \sim (0.53, -0.78, -0.35)$, $M \sim (0.13, -0.33, 0.94)$, and $N \sim (-0.84, -0.54, -0.07)$ are the maximum, intermediate and minimum variation directions in GSE coordinates, respectively. We find that the L direction is very close to the background field vector and the angle between L and the background field is only 7°, which means that the magnetic field variation is mainly along the background field similar to a compressional mode variation. The results of MVA analysis are shown in Figure 2. Data from MMS3 and MMS4 show vortex characteristics in the MN plane. The velocity in the M direction changes together with the N direction and they constitute a "circle" in Figure 2l and an irregular round shape in Figure 2m, whereas no such signature is seen for MMS1 in Figure 2k. Thus, we infer that MMS1 crossed the center of the vortex since only the velocity of the component which is perpendicular to the trajectory should vary; MMS3 and MMS4 did not cross the center of the vortex, and MMS3 was closer to the center than MMS4. This can be verified from the magnetic field data. That is, the magnetic field strength in the hole was the lowest and the duration was the longest for the observations of MMS1. The same argument can be applied to the observations of MMS3 and MMS4 (similar signatures were used in *Sundberg et al.* [2015] and *Li et al.* [2016] to verify two-dimensional circular MHs).

Figure 2d shows the current density from particle moments and the calculated electron diamagnetic current density. We estimate electron diamagnetic current from the high temporal moments measured by MMS1. The diamagnetic current is obtained from $\overrightarrow{J_P} = -\frac{(\nabla_\perp P_\perp)\times \overrightarrow{\mathbf{B}}}{B^2}$, where $\nabla_\perp P_\perp$ is the perpendicular electron pressure gradient. As MMS1 crossed the center of the vortex, we calculate the diamagnetic current (blue curve) using $Jp_i = -\frac{(P_{i+1}-P_{i-1})}{D}\frac{B_L}{B^2}$, where $P = n_e k T_\perp$ and $D = V_\perp 2\Delta t$. Here "i" represents different time instant, B_L is the magnetic field strength B along the L direction, n_e is the electron number density, k is the Boltzmann constant, $T_\perp$ is the perpendicular electron temperature, $V_\perp$ is the ion bulk velocity perpendicular to the magnetic field, and $\Delta t = 1/128$ s. The current density (red curve) is calculated from particle moments: $J = n_e e(v_i - v_e)$, where e, v_i, and v_e are the elementary Coulomb charge, the ion, and electron bulk velocities respectively. Here the ion flows can be considered as a stable background and the current is carried by electrons. It can be seen that the J is mainly contributed by the electron diamagnetic current. Here it is also clear that the electron vortex flow is from the diamagnetic drift.

4. Observations of Electron Distributions

From the measurements of FPI, we can also obtain high temporal resolution (cadence of 0.03 s) pitch angle distributions (PADs). We therefore have the opportunity to study the features of the electrons associated with the magnetic holes over a duration of 0.3 s. Electron PADs of MMS1 for event 1 are plotted in Figures 3b–33q. The perpendicular electron fluxes increased significantly for electrons with energies from 109 eV to 1024 eV inside the structure. Moreover, we find an interesting phenomenon that the fluxes of 12 eV to 26 eV electrons at 90° were almost stable and that of 34 eV to 66 eV clearly decreased. We speculate that the lower energy electrons were accelerated to the higher energy by some acceleration mechanism possibly during the size changing of the MH. A test particle simulation will be carried out in our further study. Figures 3r–3u show the phase space density (PSD) as a function of the gyroradius of electrons inside (magenta) and outside (black) the KSMH. The parallel and antiparallel directions were defined as 0–7.5° and 172.5°–180° to the field line, respectively, and the perpendicular direction were from 82.5° to 97.5°. The PSD significantly increased in the perpendicular direction for gyroradius between 1.4 km

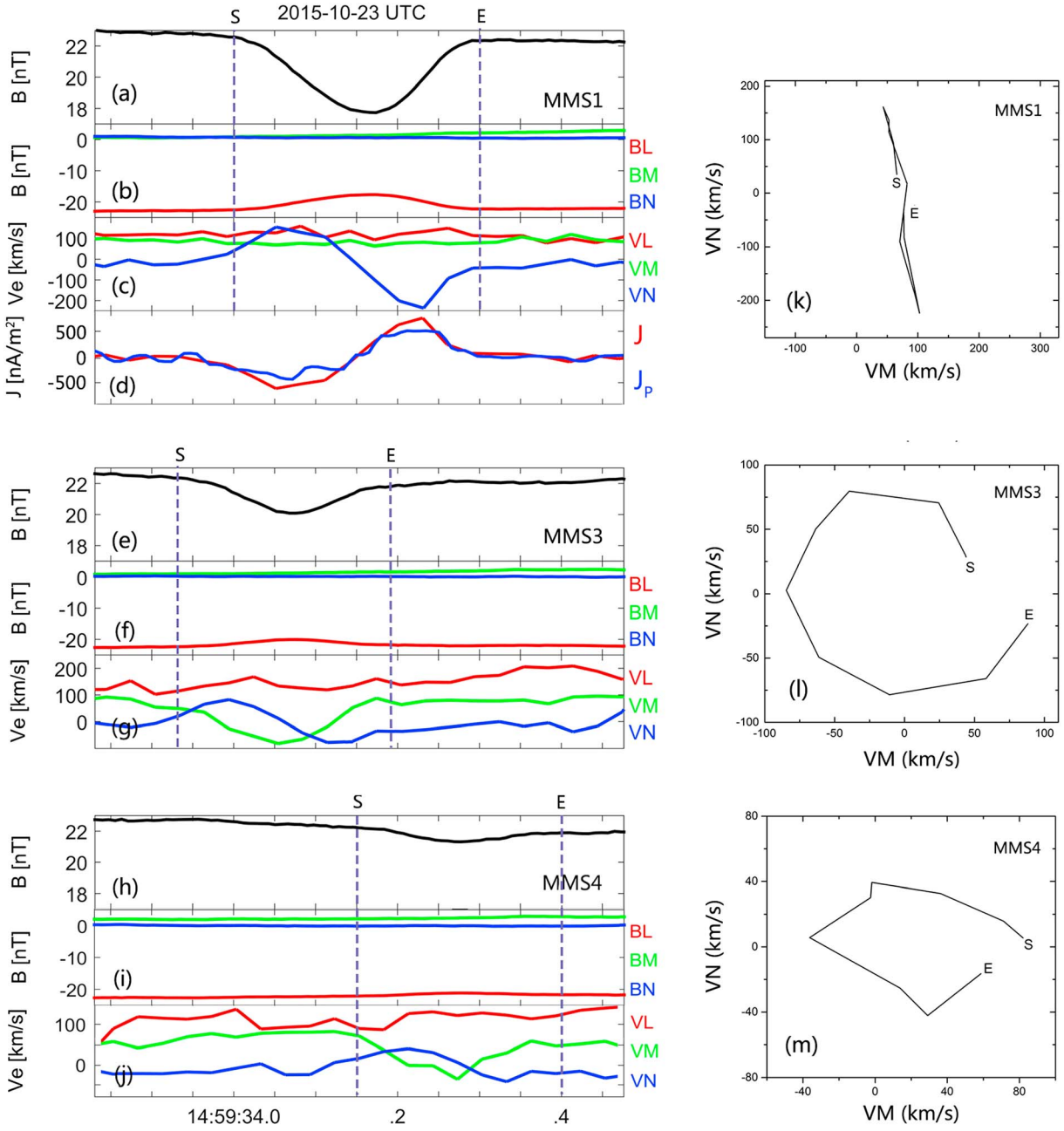

Figure 2. (a–c and e–j) The magnetic field magnitude; magnetic field, and electron bulk flow velocity of MMS1, MMS3, and MMS4 in the LMN coordinates. (d) Current density obtained from particle moments (J) and electron diamagnetic current density (J_p), respectively. (k–m) The hodograms for the electron velocities in LMN coordinates between the vertical dashed lines of Figures 1a–1c and 1e–1j, denoted as "S" (start) and "E" (end).

and 4.3 km, that is, for the electrons from 109 eV to 1024 eV that were trapped at ~90° pitch angle inside the magnetic hole. For electrons with higher energy and larger gyroradius, we suspect that they may not be trapped in the KSMHs. The increase of PSD was also found in the omnidirection as shown in Figure 3u. It is considered as the result of the ~90° trapped electrons.

5. Summary and Discussions

We report a series of KSMHs in the terrestrial magnetosheath. The main characteristics are summarized below.

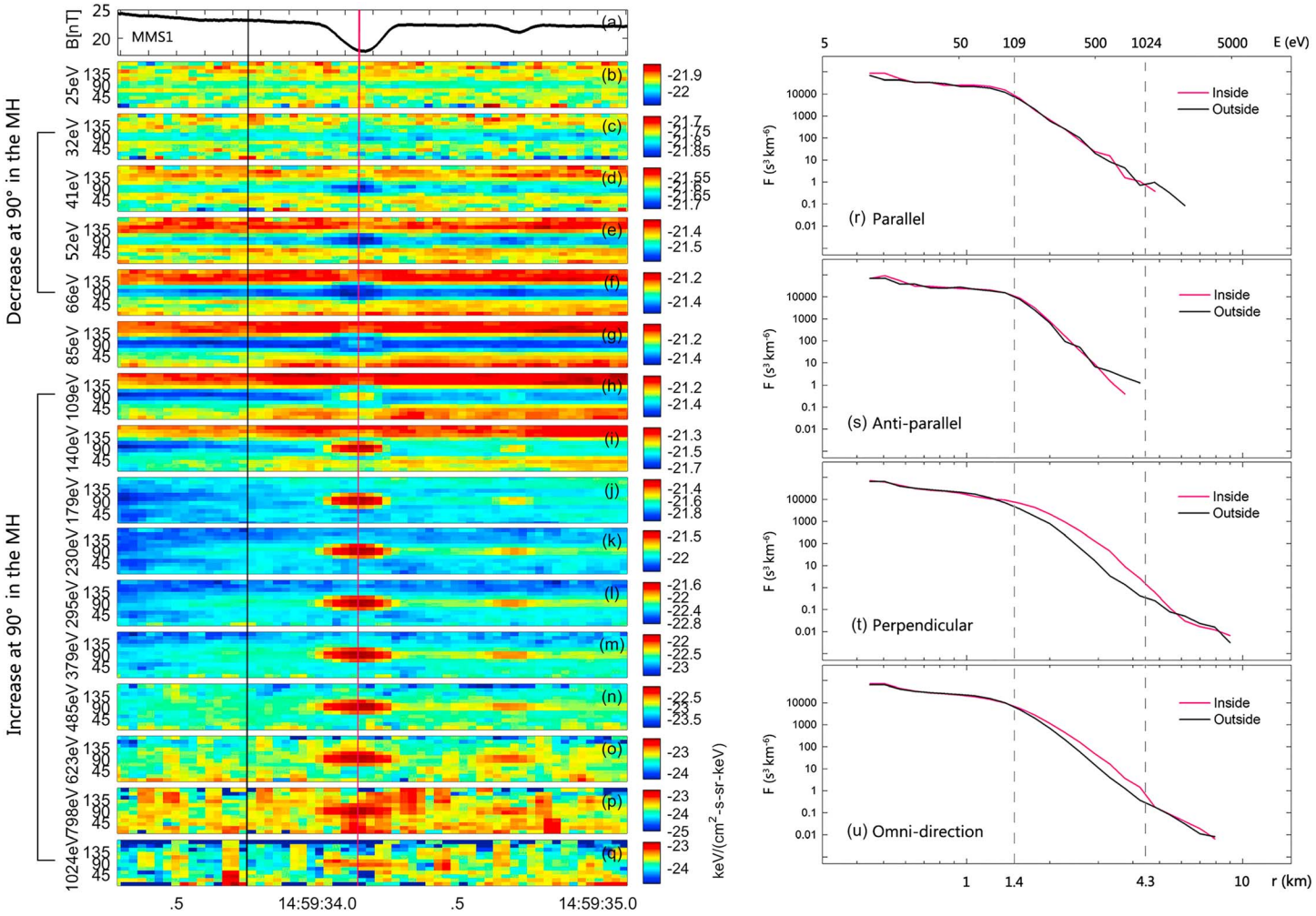

Figure 3. (a) Magnetic field strength. (b–q) Electron pitch angle distribution. (r–u) Phase space density versus electron gyroradii. The black and red lines correspond to the time marked by the black and red vertical lines in Figures 3b–3q, respectively.

1. These structures have a scale of ~10 ρ_e and are typically crossed by a spacecraft in 0.3 s.
2. The magnetic field strength decreases along the background magnetic field line; the electron number density increases inside the magnetic hole and strong electron temperature anisotropy is found inside the hole.
3. The electron flow vortex is perpendicular to the background magnetic field.
4. The calculated current density is mainly contributed by the electron diamagnetic drift, and the electron vortex flow is the diamagnetic drift flow.
5. For the 90° pitch angle electrons, the flux is steady between 12 eV and 26 eV, decreases between 34 eV and 66 eV, and significantly increases between 109 eV and 1024 eV.

Figure 4 shows a sketch of this magnetic structure deduced from the observations presented in Figures 1–3.

Two dimensional (2-D) soliton, also known as the vortex or eddy, is widely discussed in the fluid flow of geophysics. A prime example is the Great Red Spot of Jupiter, strongly swirling for some 300 years after the first observations. *Petviashvili* [1980] deduced the 2-D nonlinear equation and the 2-D soliton solution. *Flierl* [1987] investigated the isolated eddy models in the atmospheric space; monopole and dipole vortices were discussed in the study. Flow vortices are also common in space plasma fluids. Their structure and evolution become much more complicated when magnetic and electric fields exist. Plasma eddy can transport plasma across edges [e.g., *Miura*, 1984; *Hasegawa et al*., 2004], generate field-aligned currents, and have contribution to the aurora [e.g., *Birn et al*., 2004; *Keiling et al*., 2009; *Lui et al*., 2010; *Yao et al*., 2012]. Multiple scales of eddies

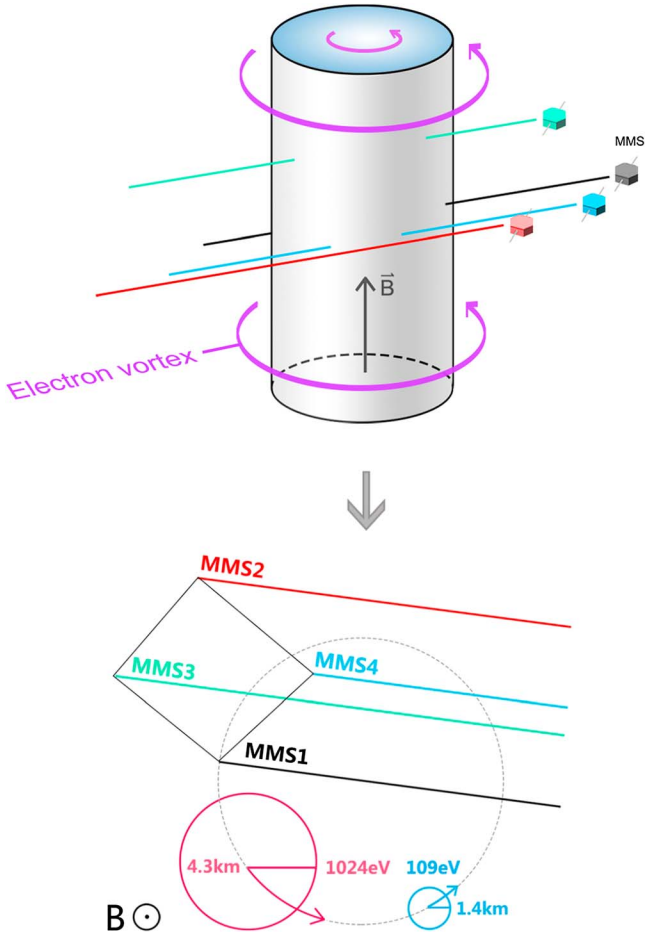

Figure 4. Sketch of MMS crossing of KSMHs which has been analyzed in Figures 1–3. Blue gradual change denotes the magnetic field magnitude.

have been found in space, such as the heliosphere [*Burlaga*, 1990], the Earth's ionosphere and magnetosphere [e.g., *Hones et al*., 1978; *Friis-Christensen et al*., 1988; *Glassmeier et al*., 1989; *Lyatsky et al*., 1999; *Murr et al*., 2002; *Motoba et al*., 2003; *Sibeck et al*., 2003; *Sundkvist et al*., 2005; *Juusola et al*., 2010; *Tian et al*., 2010., *Shi et al*., 2014; *Zhao et al*., 2016].

Ji et al. [2014] discussed the EMHD scale solitary waves. They mainly focused on solving the 1-D Korteweg de Vries (KdV) equation [*Korteweg and de Vries*, 1895] with Biermann battery effect [*Biermann*, 1950]. Furthermore, by assuming an axisymmetric perturbed magnetic field, *Li et al*. [2016] extended the 1-D KdV equation to a quasi-2-D KdV equation. In their equations 10 and 11, a slow-mode branch (magnetic field and number density out of phase) presented as the quasi-2-D solitons with the scale size ~10 ρ_e. For a solitary wave, the amplitude, wavelength, and propagating velocity are related to each other. However, in our paper, it is still difficult to determine the propagating speed for this kind of KSMHs, mainly due to two reasons. First, the separations of the four spacecraft (~20 km) are comparable to these structures size (~10 m). So it is difficult to observe the structure by all the four spacecraft. Previous multipoint spacecraft analysis methods (e.g., the timing or triangulation method [*Russell et al*., 1983; *Paschmann et al*., 1998], the MDD (minimum directional difference) method [*Shi et al*., 2005], the STD (spatiotemporal difference) method [*Shi et al*., 2006], and the MTA (multiple triangulation analysis) method [*Zhou et al*., 2006]) are based on four-point measurements, and thus they cannot be applied in our research to obtain a reliable velocity of the MH as *Yao et al*. [2016] did. Second, by plugging the observed plasma parameters into the quasi-2-D KdV equations in the traveling wave frame of *Li et al*. [2016, equation 9], we have the theoretical propagation velocity which range from 0.1 to 10 km/s in the plasma flow frame, very close to nonpropagation. In addition, by simply estimating the velocity of the KSMHs detected by three satellites (as, e.g., *Sundberg et al*. [2015] did), we find that the KSMHs may propagate with a velocity of ~10 km/s in the background plasma flow frame. However, objectively, these observed velocities show only a vague idea and the uncertainty of determining the velocity may be larger after we consider various errors. In addition, the theoretical soliton velocity is smaller than the variation of background plasma flow. Even if the observed velocities are obtained accurately, it is not suggested to do some comparison or specific calculation.

From the quasi-2-D EMHD soliton theory [*Li et al*., 2016], we know that the amplitude of an MH, $\widetilde{b}$, is proportional to v (v is a parameter characterizing the velocity of the MHs); the width L is proportional to $1/\sqrt{-v}$. Thus, we have the relation between amplitude and width $\widetilde{b} \propto \frac{1}{L^2}$. Fortunately, the time resolution of the

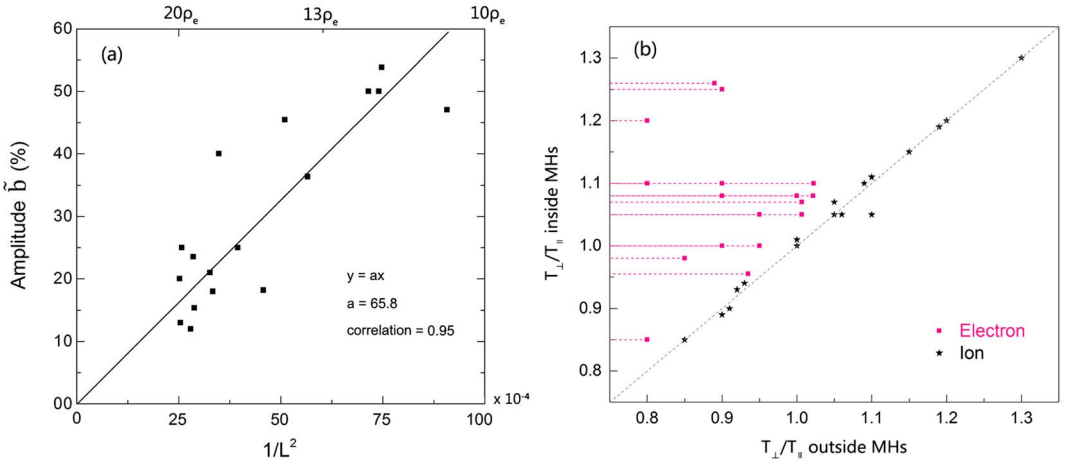

Figure 5. (a) The amplitude as a function of $1/L^2$. (b) $T_{\perp}/T_{//}$ inside MHs versus outside MHs.

FGM instrument onboard MMS is sufficient for us to get the amplitude and width of MHs. We use $(V_{\perp} \times dt)/\rho_e$ to obtain the width, where dt is the MHs duration. For instance, for the event in Figures 1–3, the width is about 20 ρ_e ($V_{\perp}$ ~ 65 km/s, dt ~ 0.24 s and ρ_e ~ 0.8 km). As 10 ρ_e is a typical scale of electron soliton, MHs size from 10 to 20 ρ_e are selected here. In total, 17 events are selected, including the event shown in Figures 1–3. The relation between $\tilde{b}$ and L of MHs is shown in Figure 5a. A straight line with equation $y = ax$ is fitted using these 17 cases. We find that $\tilde{b}$ is highly correlated with $\frac{1}{L^2}$, suggesting that the amplitude and the width of KSMHs fit well with the 2-D electron soliton theory. It should also be noted that the magnetic field perturbations in our events are less than 60%. It is in a weak nonlinear regime. For a strong magnetic field nonlinear perturbation, i.e., the magnetic field perturbation $\tilde{b} \gg$ the background field B_0, corresponding strong nonlinear theory has to be applied. Nevertheless, we need to point out that the conventional weak nonlinear soliton theory for fluids and plasmas usually only takes the convection nonlinearity into account. However, the recently developed EMHD soliton theory takes also into account the magnetic perturbation nonlinearity effect [*Ji et al*., 2014; *Li et al*., 2016; *Yao et al*., 2016].

In addition to the quasi-2-D soliton discussed above, we would like to discuss other potential explanations for our observations. The most extensively discussed mechanism in generating magnetic hole is mirror-mode instability and its additional effects, e.g., drift, electron temperature influence, finite Larmor radius, non-Maxwellian hot plasma distribution, and nonlinearity [e.g., *Feygin et al*., 2009; *Gedalin et al*., 2001; *Hasegawa*, 1969; *Hellinger et al*., 2009; *Genot et al*., 2009; *Istomin et al*., 2009; *Klimushkin and Chen*, 2006; *Pokhotelov and Pilipenko*, 1976; *Pokhotelov et al*., 2000, 2001a, 2001b; *Treumann et al*., 2004]. The instability is associated with the particles adiabatic reflection and temperature anisotropy. Thus, the size should be in the MHD scale and particles should have a strong perpendicular temperature. Figure 5b shows the temperature anisotropy inside and outside the MHs for ions and electrons. We found no clear signature of temperature anisotropy for the ions inside the MH. The structure was detected in an isotropic ion background. Therefore, the mirror-mode based on the MHD scale may not be appropriate to explain these kinetic scale structures. Instead, electrons show strong temperature anisotropy inside the structure. This may connect with the electron mirror-mode instability. However, previous theories of the instability required that the electrons temperature should be much larger than that of the ions [e.g., *Gary and Karimabadi*, 2006; *Pokhotelov et al*., 2013]. Note that in the magnetosheath, typical temperature of ions is at least 4–5 times larger than the temperature of the electrons. For the 17 events studied in this paper, the ion temperature is 4.7–8.6 times larger than the electron temperature. Perhaps further theory of electron mirror-mode without limits of this temperature condition could be developed. One possible suspect is that the KSMHs were generated in the solar wind when the electron mirror-mode condition was satisfied, and they then entered the magnetosheath and were observed by the spacecraft. The typical electron temperature is close to that of ions in the solar wind, so that there are more chances of satisfying the excitation condition of electron mirror instability. The idea should be further verified with high time resolution data in the solar wind. Recently, *Huang et al*. [2017] suggested that the KSMHs may be coherence structures generated in the sheath turbulence plasma. More works should be done to verify these possibilities.

In recent studies, KSMHs have been found in the plasma sheet by MMS spacecraft [*Gershman et al*., 2016; *Goodrich et al*., 2016]. The event in *Gershman et al*. [2016] lasted 7 s with the amplitude of ~8%, scale size 100 km to 150 km (50 to 75 ρ_e). Another observation of KSMHs was reported by *Goodrich et al*. [2016] in the bursty bulk flow braking region. The amplitude was 75% with the duration of ~5.5 s. The scale size was experientially estimated to be 1000 km (hundreds ρ_e) as the observation was lack of plasma data. Strong electric field was found in the MH edges, and $E \times$ B drift of electrons were present to be a possible generation mechanism. In a recent particle-in-cell simulation study, electron vortex magnetic hole (EVMH) within a decaying turbulence was reported by *Haynes et al*. [2015]. A diamagnetic azimuthal current was considered to be associated with the magnetic field depression. The radius of the vortex was ~5 ρ_e which fits our observations and the quasi-2-D soliton theory. We think that this simulation result may have some similar essential properties with the soliton. For example, in the quasi-2-D KdV equation, the dispersion and nonlinear terms make the vortex disperse and concentrate, respectively. When they are offsetting, the linear term will keep the vortex as a stable waveform. The electron flows contributed by diamagnetic drift, which correspond to a circular current, and thus reduce the magnetic field in the central region. These features set up a self-consistent system. In the simulation, the structure was stable over at least 100 electron gyroperiods and satisfied with the gradient drift condition. Thus, more works about the comparison between quasi-2-D soliton theory and EVMH simulation should be done.

Acknowledgments
We are very grateful to the instrumental teams of MMS for providing magnetic field and plasma data. All MMS data can be obtained from the MMS Science Data Center (https://lasp.colorado.edu/mms/sdc/public/). This work was supported by the National Natural Science Foundation of China (grants 41574157, 41322031, and 41628402). Z. H. Yao is a Marie-Curie COFUND postdoctoral fellow at the University of Liege. Cofunded by the European Union.

References

Balikhin, M. A., D. G. Sibeck, A. Runov, and S. N. Walker (2012), Magnetic holes in the vicinity of dipolarization fronts: Mirror or tearing structures, *J. Geophys. Res.*, *117*, A08229, doi:10.1029/2012JA017552.

Balikhin, M. A., R. Z. Sagdeev, S. N. Walker, O. A. Pokhotelov, D. G. Sibeck, N. Beloff, and G. Dudnikova (2009), THEMIS observations of mirror structures: Magnetic holes and instability threshold, *Geophys. Res. Lett.*, *36*, L03105, doi:10.1029/2008GL036923.

Balogh, A., M. K. Dourtghey, R. J. Forsyth, D. J. Southwood, E. J. Smith, B. T. Tsurutani, N. Murphy, and M. E. Burton (1992), Magnetic field observations during the Ulysses flyby of Jupiter, *Science*, *257*, 1515, doi:10.1126/science.257.5076.1515.

Baumgärtel, K. (1999), Soliton approach to magnetic holes, *J. Geophys. Res.*, *104*, 28,295–28,308, doi:10.1029/1999JA900393.

Bavassano-Cattaneo, M. B., C. Basile, G. Moreno, and J. D. Richardson (1998), Evolution of mirror structures in the magnetosheath of Saturn from the bow shock to the magnetopause, *J. Geophys. Res.*, *103*, 11,961, doi:10.1029/97JA03683.

Biermann, L. (1950), Über den Ursprung der Magnetfelder auf Sternen und im interstellaren Raum, *Z. Naturforsch., A: Phys. Sci.*, *5*, 65–71.

Birn, J. M., J. Raeder, Y. L. Wang, R. A. Wolf, and M. Hesse (2004), On the propagation of bubbles in the magnetotail, *Ann. Geophys.*, *22*, 1773–1786, doi:10.5194/angeo-22-1773-2004.

Burch, J. L., T. E. Moore, R. B. Torbert, and B. L. Giles (2016), Magnetospheric multiscale overview and science objectives, *Space Sci. Rev.*, *199*, 5–21, doi:10.1007/s11214-015-0164-9.

Burlaga, L. F. (1990), A heliospheric vortex street?, *J. Geophys. Res.*, *95*(A4), 4333–4336, doi:10.1029/JA095iA04p04333.

Burlaga, L. F., and J. F. Lemaire (1978), Interplanetary magnetic holes: Theory, *J. Geophys. Res.*, *83*, 5157–5160, doi:10.1029/JA083iA11p05157.

Chisham, G., S. J. Schwartz, M. A. Balikhin, and M. W. Dunlop (1999), AMPTE observations of mirror mode waves in the magnetosheath: Wavevector determination, *J. Geophys. Res.*, *104*, 437–447, doi:10.1029/1998JA900044.

Eastwood, J. P., et al. (2016), Ion-scale secondary flux ropes generated by magnetopause reconnection as resolved by MMS, *Geophys. Res. Lett.*, *43*, 4716–4724, doi:10.1002/2016GL068747.

Fazakerley, A. N., and D. J. Southwood (1994), Theory and observation of magnetosheath waves, in *Solar Wind Sources of Magnetosheath Ultra-Low-Frequency Waves, Geophys. Monogr. Ser*, vol. 81, edited by M. Engebretson, K. Takahashi, and M. Scholer, pp. 147–158, AGU, Washington, D. C.

Feygin, F. Z., Y. G. Khabazin, V. A. Simonenko, and A. A. Kondrat'ev (2009), Linear theory of slow drift mirror kinetic instability at finite electron temperature, *Geo Magn. Aeron.*, *49*, 30–41, doi:10.1134/S0016793209010046.

Flierl, G. R. (1987), Isolated eddy models in Geophysics, *Annu. Rev. Fluid Mech.*, *19*, 493–530, doi:10.1146/annurev.fl.19.010187.002425.

Friis-Christensen, E., M. A. McHenry, C. R. Clauer, and S. Vennerstrom (1988), Ionospheric traveling convection vortices observed near the polar cleft: A triggered response to sudden changes in the solar wind, *Geophys. Res. Lett.*, *15*, 253–256, doi:10.1029/GL015i003p00253.

Gary, S. P., and H. Karimabadi (2006), Linear theory of electron temperature anisotropy instabilities: Whistler, mirror, and Weibel, *J. Geophys. Res.*, *111*, A11224, doi:10.1029/2006JA011764.

Ge, Y. S., J. P. McFadden, J. Raeder, V. Angelopoulos, D. Larson, and O. D. Constantinescu (2011), Case studies of mirror-mode structures observed by THEMIS in the near-Earth tail during substorms, *J. Geophys. Res.*, *116*, A01209, doi:10.1029/2010JA015546.

Gedalin, M., Y. E. Lyubarski, M. Balikhin, and C. T. Russell (2001), Mirror modes: Non-Maxwellian distributions, *Phys. Plasmas*, *8*, 2934, doi:10.1063/1.1370362.

Genot, V., E. Budnik, P. Hellinger, T. Passot, G. Belmont, P. M. Travniek, P.-L. Sulem, E. Lucek, and I. Dandouras (2009), Mirror structures above and below the linear instability threshold: Cluster observations, fluid model and hybrid simulations, *Ann. Geophys.*, *27*, 601–615, doi:10.5194/angeo-27-601-2009.

Gershman, D. J., et al. (2016), Electron dynamics in a subproton-gyroscale magnetic hole, *Geophys. Res. Lett.*, *43*, 4112–4118, doi:10.1002/2016GL068545.

Glassmeier, K.-H., M. Hönisch, and J. Untiedt (1989), Ground-based and satellite observations of traveling magnetospheric convection twin-vortices, *J. Geophys. Res.*, *94*, 2520–2528, doi:10.1029/JA094iA03p02520.

Goodrich, K. A., et al. (2016), MMS multipoint electric field observations of small-scale magnetic holes, *Geophys. Res. Lett.*, *43*, 5953–5959, doi:10.1002/2016GL069157.

Hasegawa, A. (1969), Drift mirror instability in the magnetosphere, *Phys. Fluids*, *12*, 2642–2650, doi:10.1063/1.1692407.

Hasegawa, H., M. Fujimoto, T.-D. Phan, H. Rème, A. Balogh, M. W. Dunlop, C. Hashimoto, and R. TanDokoro (2004), Transport of solar wind into Earth's magnetosphere through rolled-up Kelvin-Helmholtz vortices, *Nature*, *430*, 755–758, doi:10.1038/nature02799.

Haynes, C. T., D. Burgess, E. Camporeale, and T. Sundberg (2015), Electron vortex magnetic holes: A nonlinear coherent plasma structure, *Phys. Plasmas*, *22*, 012309, doi:10.1063/1.4906356.

Hellinger, P., et al. (2009), Mirror instability: From quasi-linear diffusion to coherent structures, *Geophys. Res. Lett.*, *36*, L06103, doi:10.1029/2008GL036805.

Hones, E. W., Jr., G. Paschmann, S. J. Bame, J. R. Asbridge, N. Sckopke, and K. Schindler (1978), Vortices in magnetospheric plasma flow, *Geophys. Res. Lett.*, *5*(12), 1059–1062, doi:10.1029/GL005i012p01059.

Horbury, T. S., E. A. Lucek, A. Balogh, I. Dandouras, and H. Rème (2004), Motion and orientation of magnetic field dips and peaks in the terrestrial magnetosheath, *J. Geophys. Res.*, *109*, A09209, doi:10.1029/2003JA010237.

Huang, S. Y., et al. (2017), Magnetospheric Multiscale Observations of Electron Vortex Magnetic Hole in the Turbulent Magnetosheath Plasma, *Astrophys. J. Lett.*, 836, L27, doi:10.3847/20418213/aa5f50.

Istomin, Y. N., O. A. Pokhotelov, and M. A. Balikhin (2009), Mirror instability in space plasmas: Solitons and cnoidal waves, *Phys. Plasmas*, *16*, 062905, doi:10.1063/1.3153553.

Ji, X.-F., X.-G. Wang, W.-J. Sun, C.-J. Xiao, Q.-Q. Shi, J. Liu, and Z.-Y. Pu (2014), EMHD theory and observations of electron solitary waves in magnetotail plasmas, *J. Geophys. Res. Space Physics*, *119*, 4281–4289, doi:10.1002/2014JA019924.

Joy, S. P., M. G. Kivelson, R. J. Walker, K. K. Khurana, C. T. Russell, and W. R. Paterson (2006), Mirror-mode structures in the Jovian magnetosheath, *J. Geophys. Res.*, *111*, A12212, doi:10.1029/2006JA011985.

Juusola, L., K. Andreeova, O. Amm, K. Kauristie, S. E. Milan, M. Palmroth, and N. Partamies (2010), Effects of a solar wind dynamic pressure increase in the magnetosphere and in the ionosphere, *Ann. Geophys.*, *28*(10), 1945–1959, doi:10.5194/angeo-28-1945-2010.

Kaufmann, R. L., J.-T. Horng, and A. Wolfe (1970), Large-amplitude hydromagnetic waves in the inner magnetosheath, *J. Geophys. Res.*, *75*(25), 4666–4676, doi:10.1029/JA075i025p04666.

Keiling, A., et al. (2009), Substorm current wedge driven by plasma flow vortices: THEMIS observations, *J. Geophys. Res.*, *114*, A00C22, doi:10.1029/2009JA014114.

Klimushkin, D. Y., and L. Chen (2006), Eigenmode stability analysis of drift-mirror modes in nonuniform plasmas, *Ann. Geophys.*, *24*, 2435–2439, doi:10.5194/angeo-24-2435-2006.

Korteweg, D. J., and G. de Vries (1895), On the change of form of long waves advancing in a rectangular canal and on a new type of long stationary waves, *Philos. Mag.*, *39*, 422–443, doi:10.1080/14786449508620739.

Li, Z.-Y., W.-J. Sun, X.-G. Wang, Q.-Q. Shi, C.-J. Xiao, Z.-Y. Pu, X.-F. Ji, S.-T. Yao, and S.-Y. Fu (2016), An EMHD soliton model for small-scale magnetic holes in magnetospheric plasmas, *J. Geophys. Res. Space Physics*, *121*, 4180–4190, doi:10.1002/2016JA022424.

Lucek, E. A., M. W. Dunlop, A. Balogh, P. Cargill, W. Baumjohann, E. Georgescu, G. Haerendel, and K.-H. Fornacon (1999), Mirror mode structures observed in the dawn-side magnetosheath by Equator-S, *Geophys. Res. Lett.*, *26*, 2159, doi:10.1029/1999GL900490.

Lui, A. T. Y., E. Spanswick, E. F. Donovan, J. Liang, W. W. Liu, O. LeContel, and Q.-G. Zong (2010), A transient narrow poleward extrusion from the diffuse aurora and the concurrent magnetotail activity, *J. Geophys. Res.*, *115*, A10210, doi:10.1029/2010JA015449.

Lyatsky, W. B., G. J. Sofko, A. V. Kustov, D. Andre, W. J. Hughes, and D. Murr (1999), Traveling convection vortices as seen by the SuperDARN HF radars, *J. Geophys. Res.*, *104*(A2), 2591–2601, doi:10.1029/1998JA900007.

Miura, A. (1984), Anomalous transport by magnetohydrodynamic Kelvin-Helmholtz instabilities in the solar wind-magnetosphere interaction, *J. Geophys. Res.*, *89*, 801–818, doi:10.1029/JA089iA02p00801.

Motoba, T., T. Kikuchi, T. Okuzawa, and K. Yumoto (2003), Dynamical response of the magnetosphere-ionosphere system to a solar wind dynamic pressure oscillation, *J. Geophys. Res.*, *108*(A5), 1206, doi:10.1029/2002JA009696.

Murr, D. L., W. J. Hughes, A. S. Rodger, E. Zesta, H. U. Frey, and A. T. Weatherwax (2002), Conjugate observations of traveling convection vortices: The field-aligned current system, *J. Geophys. Res.*, *107*(A10), 1306, doi:10.1029/2002JA009456.

Nowada, M., J.-H. Shue, C.-H. Lin, T. Sakurai, D. G. Sibeck, V. Angelopoulos, C. W. Carlson, and H.-U. Auster (2009), Alfve'nic plasma velocity variations observed at the inner edge of the low-latitude boundary layer induced by the magnetosheath mirror mode waves: A THEMIS observation, *J. Geophys. Res.*, *114*, A07208, doi:10.1029/2008JA014033.

Paschmann, G., A. N. Fazakerley, and S. J. Schwartz (1998), Moments of plasma velocity distributions, in *Analysis Methods for Multi-Spacecraft Data*, pp. 125–158, ISSI SA Publications Division, Noordwijk, Netherlands.

Petviashvili, V. I. (1980), Red spot of Jupiter and drift soliton in a plasma, *JETP Lett., Engl. Transl.*, *32*, 619.

Pokhotelov, O. A., and V. A. Pilipenko (1976), Contribution to the theory of the drift-mirror instability of the magnetospheric plasma, *Geomagn. Aeron.*, *16*, 296.

Pokhotelov, O. A., M. A. Balikhin, H. S. Alleyne, and O. G. Onishchenko (2000), Mirror instability with finite electron temperature effects, *J. Geophys. Res.*, *105*, 2393, doi:10.1029/1999JA900351.

Pokhotelov, O. A., M. A. Balikhin, R. A. Treumann, and V. P. Pavlenko (2001a), Drift mirror instability revisited: 1. Cold electron temperature limit, *J. Geophys. Res.*, *106*, 8455–8464, doi:10.1029/2000JA000069.

Pokhotelov, O. A., O. G. Onishchenko, M. A. Balikhin, R. A. Treumann, and V. P. Pavlenko (2001b), Drift mirror instability in space plasmas: 2. Nonzero electron temperature effects, *J. Geophys. Res.*, *106*, 13,237–13,246, doi:10.1029/2000JA000310.

Pokhotelov, O. A., O. G. Onishchenko, and L. Stenflo (2013), Physical mechanisms for electron mirror and field swelling modes, *Phys. Scr.*, *87*(6), 065,303, doi:10.1088/0031-8949/87/06/065303.

Pollock, C., et al. (2016), Fast plasma investigation for magnetospheric multiscale, *Space Sci. Rev.*, *199*, 331, doi:10.1007/s11214-016-0245-4.

Roytershteyn, V., H. Karimabadi, and A. Roberts (2015), Generation of magnetic holes in fully kinetic simulations of collisionless turbulence, *Phil. Trans. R. Soc. A*, *373*, 20,140,151, doi:10.1098/rsta.2014.0151.

Russell, C. T., M. M. Mellott, E. J. Smith, and J. H. King (1983), Multiple spacecraft observations of interplanetary shocks: Four spacecraft determination of shock normals, *J. Geophys. Res.*, *88*(A6), 4739–4748, doi:10.1029/JA088iA06p04739.

Russell, C. T., W. Riedler, K. Schwingenshuh, and Y. Yeroshenko (1987), Mirror instability in the magnetosphere of Comet Halley, *Geophys. Res. Lett.*, *14*, 644, doi:10.1029/GL014i006p00644.

Russell, C. T., et al. (2016), The magnetospheric multiscale magnetometers, *Space Sci. Rev.*, doi:10.1007/s11214-014-0057-3.

Shi, Q. Q., C. Shen, Z. Y. Pu, M. W. Dunlop, Q.-G. Zong, H. Zhang, C. J. Xiao, Z. X. Liu, and A. Balogh (2005), Dimensional analysis of observed structures using multipoint magnetic field measurements: Application to Cluster, *Geophys. Res. Lett.*, *32*, L12105, doi:10.1029/2005GL022454.

Shi, Q. Q., C. Shen, M. W. Dunlop, Z. Y. Pu, Q.-G. Zong, Z. X. Liu, E. Lucek, and A. Balogh (2006), Motion of observed structures calculated from multi-point magnetic field measurements: Application to Cluster, *Geophys. Res. Lett.*, *33*, L08109, doi:10.1029/2005GL025073.

Shi, Q. Q., et al. (2009), Spatial structures of magnetic depression in the Earth's high-altitude cusp: Cluster multipoint observations, *J. Geophys. Res.*, *114*, A10202, doi:10.1029/2009JA014283.
Shi, Q. Q., et al. (2014), Solar wind pressure pulse-driven magnetospheric vortices and their global consequences, *J. Geophys. Res. Space Physics*, *119*, 4274–4280, doi:10.1002/2013JA019551.
Sibeck, D. G., N. B. Trivedi, E. Zesta, R. B. Decker, H. J. Singer, A. Szabo, H. Tachihara, and J. Watermann (2003), Pressure-pulse interaction with the magnetosphere and ionosphere, *J. Geophys. Res.*, *108*(A2), 1095, doi:10.1029/2002JA009675.
Sonnerup, B. U. O., and M. Scheible (1998), Minimum and maximum variance analysis, in *Analysis Methods for Multi-Spacecraft Data*, edited by G. Paschmann and P. W. Daly, pp. 185–220, Eur. Space Agency, Bern.
Soucek, J., E. Lucek, and I. Dandouras (2008), Properties of magnetosheath mirror modes observed by Cluster and their response to changes in plasma parameters, *J. Geophys. Res.*, *113*, A04203, doi:10.1029/2007JA012649.
Southwood, D. J., and M. G. Kivelson (1993), Mirror instability: 1. Physical mechanism of linear instability, *J. Geophys. Res.*, *98*(A6), 9181–9187, doi:10.1029/92JA02837.
Stasiewicz, K. (2004), Theory and observations of slow-mode solitons in space plasmas, *Phys. Rev. Lett.*, *93*, 125,004, doi:10.1103/PhysRevLett.93.125004.
Sun, W. J., et al. (2012), Cluster and TC-1 observation of magnetic holes in the plasma sheet, *Ann. Geophys.*, *30*, 583–595, doi:10.5194/angeo-30-583-2012.
Sundberg, T., D. Burgess, and C. T. Haynes (2015), Properties and origin of subproton-scale magnetic holes in the terrestrial plasma sheet, *J. Geophys. Res. Space Physics*, *120*, 2600–2615, doi:10.1002/2014JA020856.
Sundkvist, D., V. Krasnoselskikh, P. K. Shukla, A. Vaivads, M. André, S. Buchert, and H. Rème (2005), In situ multi-satellite detection of coherent vortices as a manifestation of Alfvénic turbulence, *Nature*, *436*, 825–828, doi:10.1038/nature03931.
Tian, A. M., Q. G. Zong, Y. F. Wang, Q. Q. Shi, S. Y. Fu, and Z. Y. Pu (2010), A series of plasma flow vortices in the tail plasma sheet associated with solar wind pressure enhancement, *J. Geophys. Res.*, *115*, A09204, doi:10.1029/2009JA014989.
Treumann, R. A., C. H. Jaroschek, O. D. Constantinescu, R. Nakamura, O. A. Pokhotelov, and E. Georgescu (2004), The strange physics of low frequency mirror mode turbulence in the high temperature plasma of the magnetosheath, *Nonlinear Processes Geophys.*, *11*, 647–657, doi:10.5194/npg-11-647-2004.
Tsurutani, B. T., E. Smith, R. Anderson, K. Ogilvie, J. Scudder, D. Baker, and S. Bame (1982), Lion roars and nonoscillatory drift mirror waves in the magnetosheath, *J. Geophys. Res.*, *87*(A8), 6060–6072, doi:10.1029/JA087iA08p06060.
Tsurutani, B. T., I. G. Richardson, R. P. Lepping, R. D. Zwickl, D. E. Jones, and E. J. Smith (1984), Drift mirror Mode waves in the distant (X = 200 *Re*) magnetosheath, *Geophys. Res. Lett.*, *11*, 1102, doi:10.1029/GL011i010p01102.
Turner, J. M., L. F. Burlaga, N. F. Ness, and J. F. Lemaire (1977), Magnetic holes in the solar wind, *J. Geophys. Res.*, *82*, 1921–1924, doi:10.1029/JA082i013p01921.
Violante, L., M. B. Bavassano Cattaneo, G. Moreno, and J. D. Richardson (1995), Observations of mirror waves and plasma depletion layer upstream of Saturn's magnetopause, *J. Geophys. Res.*, *100*, 12,047, doi:10.1029/94JA02703.
Walker, S. N., M. A. Balikhin, and M. Dunlop (2002), Mirror structures in the magnetosheath: 3D structures on plane waves, *Adv. Space Res.*, *30*, 2745–2750, doi:10.1016/S0273-1177(02)80400-8.
Walker, S. N., F. Sahraoui, M. A. Balikhin, G. Belmont, J. L. Pincon, L. Rezeau, H. Alleyne, N. Cornilleau-Wehrlin, and M. Andre (2004), A comparison of wave mode identification techniques, *Ann. Geophys.*, *22*, 3021–3032, doi:10.5194/angeo-22-3021-2004.
Winterhalter, D., M. Neugebauer, B. E. Goldstein, E. J. Smith, S. J. Bame, and A. Balogh (1994), Ulysses field and plasma observations of magnetic holes in the solar wind and their relation to mirror-mode structures, *J. Geophys. Res.*, *99*, 23,371–23,381, doi:10.1029/94JA01977.
Xiao, T., et al. (2010), Cluster-C1 observations on the geometrical structure of linear magnetic holes in the solar wind at 1 AU, *Ann. Geophys.*, *28*, 1695–1702, doi:10.5194/angeo-28-1695-2010.
Xiao, T., Q. Q. Shi, and W. J. Sun (2011), Cluster observations of magnetic holes near the interplanetary current sheets at 1 AU, in 2011 30th URSI Gen. Ass. Sci. Symp., pp. 1–3.
Xiao, T., Q. Q. Shi, A. M. Tian, W. J. Sun, H. Zhang, X. C. Shen, and A. M. Du (2014), Plasma and magnetic-field characteristics of magnetic decreases in the solar wind at 1 AU: Cluster-C1 observations, *Sol. Phys.*, *289*(8), 3175–3195, doi:10.1007/s11207-014-0521-y.
Yao, S. T., et al. (2016), Propagation of small size magnetic holes in the magnetospheric plasma sheet, *J. Geophys. Res. Space Physics*, *121*, 5510–5519, doi:10.1002/2016JA022741.
Yao, Z. H., et al. (2012), Substorm current wedge formation: THEMIS observations, *J. Geophys. Res.*, *39*, L13102, doi:10.1029/2012GL052055.
Zhang, T. L., et al. (2008), Characteristic size and shape of the mirror mode structures in the solar wind at 0.72 AU, *Geophys. Res. Lett.*, *35*, L10106, doi:10.1029/2008GL033793.
Zhang, T. L., W. Baumjohann, C. T. Russell, L. K. Jian, C. Wang, J. B. Cao, M. Balikhin, X. Blanco-Cano, M. Delva, and M. Volwerk (2009), Mirror mode structures in the solar wind at 0.72 AU, *J. Geophys. Res.*, *114*, A10107, doi:10.1029/2009JA014103.
Zhao, H. Y., et al. (2016), Magnetospheric vortices and their global effect after a solar wind dynamic pressure decrease, *J. Geophys. Res. Space Physics*, *121*, 1071–1077, doi:10.1002/2015JA021646.
Zhou, X.-Z., Q.-G. Zong, J. Wang, Z. Y. Pu, X. G. Zhang, Q. Q. Shi, and J. B. Cao (2006), Multiple triangulation analysis: Application to determine the velocity of 2-D structures, *Ann. Geophys.*, *24*, 3173–3177, doi:10.5194/angeo-24-3173-2006.